Journal of Solid State Chemistry 183 (2010) 1141–1149

Contents lists available at ScienceDirect

Journal of Solid State Chemistry

journal homepage: www.elsevier.com/locate/jssc

Application of Brazilian kaolinite clay as adsorbent to removal of U(VI) from aqueous solution: Kinetic and thermodynamic of cation–basic interactions

Denis L. Guerra [a,*], Victor L. Leidens [a], Rúbia R. Viana [a], Claudio Airoldi [b]

[a] Universidade Federal de Mato Grosso, UFMT, Centro de Recursos Minerais, Cuiabá 78060 900, Mato Grosso, Brazil
[b] Chemistry Institute, State University of Campinas, P.O. Box 6154, 13084-971 Campinas, São Paulo, Brazil

ARTICLE INFO

Article history:
Received 20 November 2009
Received in revised form
27 February 2010
Accepted 13 March 2010
Available online 18 March 2010

Keywords:
Kaolinite
Uranyl
Adsorption
Calorimetry
Thermodynamic

ABSTRACT

The compound N^1-[3-(trimethoxysilyl)propyl]diethylenetriamine was anchored onto Amazon kaolinite surface by heterogeneous route. The modified and natural kaolinite samples were characterized by transmission electron microscopy, scanning electron microscopic, X-ray diffraction, and nuclear magnetic nuclei of ^{29}Si and ^{13}C. The well-defined peaks obtained in the ^{13}C NMR spectrum in the 5.0–62.1 ppm region confirmed the attachment of organic functional groups as pendant chains bonded into the porous clay. The ability of these materials to remove U(VI) from aqueous solution was followed by a series of adsorption isotherms adjusted to a Sips equation at room temperature and pH 4.0. The kinetic parameters analyzed by the Lagergren and Elovich models gave a good fit for a pseudo-second order reaction with k_2 values 16.0 and 25.1 mmol g^{-1} min^{-1} ranges for natural and modified kaolinite clays, respectively. The energetic effects caused by metal ion adsorption were determined through calorimetric titrations.

1. Introduction

An especially interesting area is the control of toxic/heavy metal ions in soils and aqueous systems [1,2]. Various conventional and non-conventional adsorbents have been explored for removal of different metal ions from aqueous. For example, materials containing micropores and macropores, such as pillared and intercalated clays, are often employed in such operations. In particular, kaolinite and smectite group clay minerals have been successfully explored in adsorption procedures [1–4]. Adsorption and ion exchange processes are the most useful methods to remove them, by exploring the availability of different kinds of adsorbents associated with convenient procedures for obtaining high efficiency [5,6]. Certain factors influence the amount of metal ions being adsorbed by mineral substrates: pH, nature of the adsorbent, adsorbent dose, initial metal ion concentration, ionic strength, and presence of competing ions [7]. A large number of different adsorbent materials containing a variety of attached chemical functional groups have been reported for this purpose. In recent years, special attention has been focused on the use of natural clay adsorbents as an alternative to replace the conventional adsorbents. A potential important adsorbent of uranyl is layered silicates like kaolinite [7,8]. Kaolinite is an important phyllosilicate with fibrous morphology in industrial applications due to its physical and chemical properties [8].

This investigation reports the use of original and modified kaolinite clays as alternative absorbents for extraction of uranyl ion, under environmental conditions, uranium occurs in the hexavalent form as the mobile aqueous uranyl ion (UO_2^{2+}), which are commonly present in waters from a variety of sources and industrial effluents. For this propose, the adsorption isotherms of U(VI) from aqueous medium at room temperature were explored, bearing in mind the influence of different parameters such as solution metal concentration and contact time. The quick adsorption process reached the equilibrium before 10 and 20 min for KLT_{MPDET} (modified clay) and KLT (natural clay), respectively. Amazon kaolinite clay sample has been chemically modified with N^1-[3-(trimethoxysilyl)propyl]diethylenetriamine (MPDET) using the heterogeneous route [9]. The performance in adsorbing uranyl cation from natural water under dynamic flow (column) conditions was also studied and the results confirmed the batch experiments. The kinetic of adsorption was studied through the Lagergren and Elovich models. From calorimetric determinations the quantitative thermal effects for all these cation/basic center interactions gave exothermic enthalpy, negative Gibbs free energy, and positive entropy. These thermodynamic data confirmed the energetically favorable condition of such interactions at the solid/liquid interface for all systems.

* Corresponding author. Fax: +55 19 33429407.
E-mail addresses: denis@cpd.ufmt.br, dlguerra@pq.cnpq.br (D.L. Guerra).

0022-4596/$ - see front matter © 2010 Published by Elsevier Inc.
doi:10.1016/j.jssc.2010.03.021

2. Experimental section

2.1. Raw material

The clay sample used in this investigation was obtained from the Tabatinga area, Amazonas state, North of Brazil, Amazon region. A natural kaolinite sample, named KLT, with less than 2 μm particles, was separated by sedimentation. The cation exchange capacity (CEC) of KLT was followed by the ammonium acetate method [10] with a concentration of 2.0 mol dm^{-3} at pH 8.0, giving 15.0 meq./100 g of clay.

2.2. Organofunctionalization of kaolinite clay

In the first step, *n*-dodecylamine was mixed with deionized water and ethanol and allowed to stir continuously for 45 min. In the second step, approximately 5 g of original kaolinite sample (KLT) was added to the mixture and the stirring was continued for 50 min. During this time period the silylating agent (MPDET) was added dropwise to form the final hybrid material, which is called KLT_{MPDET}. After addition of silylating agent, the resulting mixture was further stirred for 20 h at 291 ± 1 K. At the end of the above process, the material was centrifuged, washed with deionized water and air dried at room temperature for 30 h. The final material was subjected to Soxhlet extraction for 72 h using ethanol as solvent [9].

2.3. Characterization methods

Transmission electron microscopy (TEM) images were recorded in a JEM 3010 URP microscope at LNLS/Brazil with an accelerating voltage of 300 kV. The samples were prepared by placing a drop of a suspension of particles dispersed in isopropanol onto a carbon-coated copper grid.

The natural and modified kaolinite clays were analyzed by scanning electron microscopy (SEM) in JEOL microscope, model JEOL JSM 6360LV, using an acceleration voltage of 15 kV, and magnification ranging from 300- to 3000-fold.

X-ray powder diffraction (XRD) patterns were recorded with Philips PW 1050 diffactometer using Cu$K\alpha$ (0.154 nm) radiation in the region in the between 2° and 65° (2θ) at a speed of 2° min^{-1} and in steps of 0.050°.

Nuclear magnetic resonance spectra of the samples were obtained on a Brucker AC 300/P spectrometer at room temperature. For each run, approximately 1 g of each solid sample was compacted into a 7 mm zirconium oxide rotor. The measurements were obtained at frequencies of 59.63 and 75.47 MHz, for silicon and carbon atoms, respectively, with a magic angle spinning of 4 kHz. In order to increase the signal to noise ratio of the solid-state spectra, the CP/MAS technique was used. ^{29}Si and ^{13}C CP/MAS spectra were obtained with pulse repetitions of 3 s for both nuclei and contact times of 1 and 3 ms, respectively.

The elemental analysis (%C, %N, and %S) was determined on a Perkin-Elmer 2400 Series II microelemental analyzer, and at least two independent determinations were performed for modified clay sample.

Brunauer–Emmett–Teller (BET) [11] surface area, pore diameter, and pore volume were obtained from nitrogen adsorption/desorption in a Micromeritics ASAP 2000 BET surface analyzer system. The mesopore size distribution was obtained by applying the Barret–Joyner–Halenda (BJH) [12] method to the adsorption branch of the isotherm.

2.4. Batch adsorption study

The adsorption experiments were performed through the batchwise method by suspending a series of 20 mg samples of the solid, in 20.0 cm^3 aqueous solutions of cations at concentrations varying from 1.25×10^{-2} to 2.50×10^{-2} mmol dm^{-3}, under orbital stirring for 24 h at 298 ± 1 K [13,14]. Profiles of the obtained adsorption isotherms represented by the number of moles adsorbed (N_f), versus the number of moles at equilibrium per volume of solution (C_S), for series of isotherms, revealed that the adsorption process conforms to the Sips model. Sips [15] combined the Langmuir [16] and Freundlich [17] equations (Eq. (1)):

$$N_f = \frac{N_S K_S C_S^{1/n}}{1 + K_S C_S^{1/n}} \quad (1)$$

where C_S is the concentration of the solution at equilibrium (mol dm^{-3}), N_f is defined as before (mmol g^{-1}) and N_S is the maximum number of moles of adsorbed per gram of the adsorbent (mmol g^{-1}), which also depends upon the number of adsorption sites, K_S is the equilibrium constant, and n is the Freundlich exponent. Firstly, the effect of pH on adsorption for two clay samples was evaluated by varying this parameter over the range from 1.0 to 5.0, with addition of 0.10 mol dm^{-3} of nitric acid or sodium hydroxide. The pH of the solutions was measured using a pH/ion analyzer, model 450M. In the investigation of the influence of contact time in the adsorption process, the kinetic parameters were analyzed by Lagergren pseudo first-second-order [18] and Elovich [19] models.

Uranyl concentrations in the supernatant were determined using the kinetic phosphorescence analyzer KPA-10. The uranyl samples and reference are excited by firing the nitrogen laser at 337 nm. This excites the dye laser to produce an excitation wavelength of 420 nm. Each analysis is a repetition of 50 cycles. A 3 ns laser pulse initiates each cycle.

2.5. Column adsorption study

A glass column of 15.0 cm length and 0.50 cm internal diameter containing a porous sintered glass disk at the bottom and a Teflon stopcock was packed with 1.00 g of kaolinite samples, which occupied 5.0 cm^3 of this column. Above the packing material, the column was fulfilled individually with 2.0×10^{-2} mmol dm^3 of the U(VI) at pH 4.0. The effluent column flow-rate was adjusted to 3.5 cm^3 min^{-1} and the height of the metallic ion above the phyllosilicate adsorbents, was kept constant by feeding the column with a peristaltic pump. The column effluents were collected at each 50.0 cm^3 and metallic ions contents were determined using a Flame Atomic Absorption Spectrometry (Analyst 200, Perkin-Elmer).

2.6. Thermodynamic study

The thermal effects from metal ion interacting on natural and modified kaolinite samples were followed by calorimetric titrations using an isothermal calorimeter, Model LKB 2277, from thermometric. In this titration, the metallic solution is added to a suspension of about 20 mg of the phyllosilicate sample in 2.0 cm^3 of water, under stirring at 298 ± 1 K. A series of increments of 10 μL of metallic solutions were added to the metal ion-phyllosilicate to obtain the thermal effect of interaction (Q_t). Two other titrations are needed to complete the full experiment: (i) the thermal effect due to hydration of the silicate sample (Q_h), which normally gives a null value and (ii) and the dilution effect of metallic solution in water, without sample in the vessel (Q_d).

The resulting thermal effect is given by the following equation: $\Sigma Q_r = \Sigma Q_t - \Sigma Q_d$ [20,21]. The molar enthalpy (ΔH) of the interaction process can be calculated by the expression $\Delta H = \Delta_{int} h N_S$. The Gibbs free energy can be calculated by the equation $\Delta G = RT \ln K_S$ equation, the entropy is finally calculated from $\Delta G = \Delta H - T\Delta S$ [22].

3. Results and discussion

3.1. Characterization of materials

The scanning electron microscopy and the transmission electron microscopy (TEM) results of pristine kaolinite clay and chemically modified kaolinite clay are shown in Fig. 1d, was analyzed by SEM and TEM. Natural Amazon kaolinite presented abundant stacks or 'books', straight or curved formed by crystal of perfect pseudohexagonal morphology, as confirmed by TEM image (Fig. 1c). The presence of agglomerated particles of nanodimensions was also noted in the natural kaolinite sample. Small aggregates of rounded crystal coexisted with hexagonal kaolinite particles with particle size mostly smaller than 5.0 μm, as illustrated in Fig. 1a. This morphology was similar to that described by Keller [23] for weathered hydrothermal kaolin samples, with particles and 'books' randomly oriented. In general, kaolinite crystals of large size ($>1.0\,\mu m$) showed pseudohexagonal form and well defined edges, whereas the edges of crystals of small sizes were rounded. This morphology was similar to that described by Zbik and Smart [24] for North Queensland kaolinite particles. Some crystals were also detected by AFM studies. Fig. 1b displays the SEM micrographs of the organofunctionalized kaolinite. In this case, the particles are apparently smaller in size and are constituted of disordered, thin sheet particle aggregates. One can conclude that functionalization promotes the formation of disordered and less cohesive aggregates, probably due to reduction of the edge-to-edge and face-to-face interactions, as confirmed by TEM image (Fig. 1d). The crystals present some fissures and holes, which indicates the presence of a macroporous structure.

The X-ray diffraction patterns for samples showed at low angle the characteristic reflection related to the kaolinite clay samples [25]. The determination of the total mineralogical composition of the pristine natural clay sample was carried out on oriented mounts, exhibiting mainly kaolinite, quartz, and goethite, as shown in Fig. 2a. After intercalation process the kaolinite presented, as expected, an increase in basal distance, changing the d_{001} value from 0.728 nm for natural kaolinite to 2.130 nm for the intercalated form (Fig. 2a and b). It was also observed that the KLT sample presents a slightly broader and less intense peak, in comparison with KLT_{MPDET}, a behavior that could be attributed to differences in the degree of crystallinity [25]. This fact confirms that the organic–inorganic precursor was successfully intercalated into the interlayer space with the MPDET units perpendicularly oriented to the phyllosilicate layer. The great influence of the number of MPDET ions on the surface and on the constitution and distribution of the ions has been previously reported. The mass fraction of intercalated material can be estimated as the relative intensities of the reflection originating from the 'unchanged' and the 'expanded' layers. In the intercalated sample, the degree of intercalation reaction could be estimated as 88.03%. This indicates that the MPDET molecules arrange in monolayers between the phyllosilicate layers.

Nuclear magnetic resonance in the solid-state is a technique to give valuable information about the bonding of the pendant chains anchored on an inorganic backbone. For this purpose silicon and carbon nuclei were examined in order to better characterize the natural and modified kaolinite clays. The ^{29}Si NMR spectra of the natural and modified kaolinite clays, presented in Fig. 3a and b, respectively, shows a series of typical phyllosilicate signals that correspond to (i) $Si(OSi)_4$, Q^4, at 102.0 ppm, (ii) $Si(OSi)_3OH$, Q^3, at −92.0 ppm while (iii) a possible weak broad shoulder at −91.0 ppm could be assigned to Q^2, $Si(OSi)_2(OH)_2$. Two other peaks found at −72.0 and −58.0 ppm were assigned to $RSi(OSi)_3$ (T^3) and $RSi(OSi)(OH)_2$ (T^2) signals, respectively. These signals originate from the structural units related to the presence of an organic part covalently bonded to the inorganic backbone silicate structure. The relative intensity of the peak for Q^3 was higher in comparison to Q^4 species and this is in agreement with similar observations in the case of hybrid materials. The covalent silylating agent attachment as tripoid bonding on inorganic structure is confirmed by the presence of T^3 species, which assigned

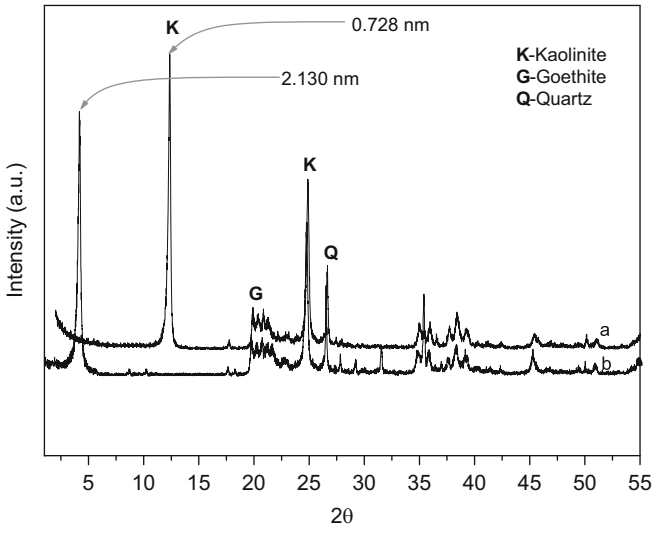

Fig. 2. X-ray diffraction patterns for unmodified and modified kaolinite samples: KLT (a) and KLT_{MPDET} (b).

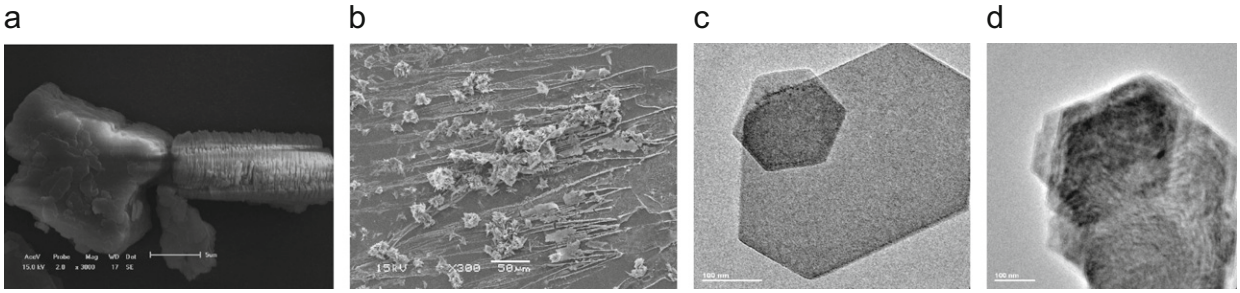

Fig. 1. Morphology of the natural and modified kaolinite samples: SEM of KLT (a) and SEM of KLT_{MPDET} (b) and TEM of KLT (c), and TEM of KLT_{MPDET} (d).

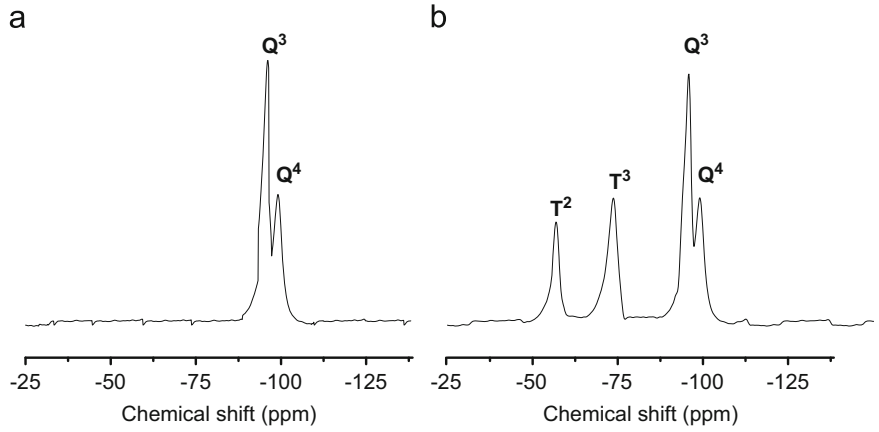

Fig. 3. ^{29}Si MAS NMR spectra of unmodified and modified kaolinite samples: KLT (a) and KLT_{MPDET} (b).

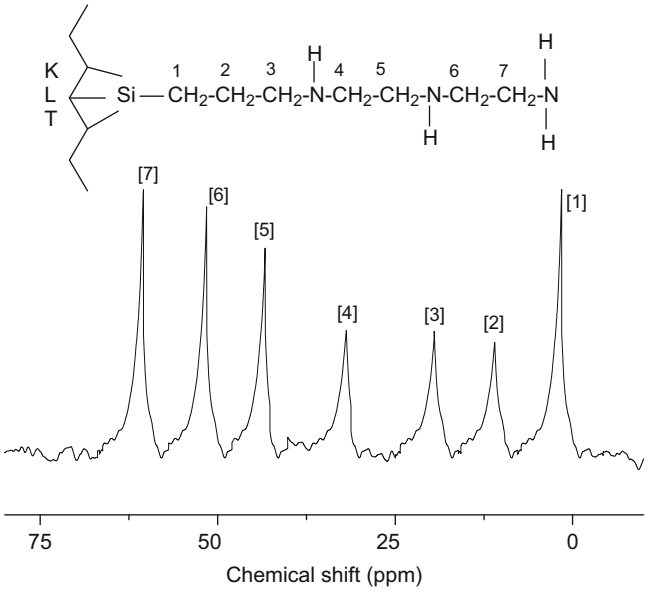

Fig. 4. ^{13}C MAS NMR spectrum of modified kaolinite sample, KLT_{MPDET}.

sequence of organic carbon atoms chain, without any template agent, is supported by ^{13}CNMR [26].

The hybrid material showed well-resolved peaks positioned at 5.0, 13.0, and 20.0 ppm for the spacer propyl chain carbon atoms attached to silicate. Other carbon atoms, numbered as in the proposed structure, were observed at 37.0 and 46.0 ppm, respectively, assigned to C_4 and C_5, and other peaks at 58.0 and 62.1 ppm were assigned to C_6 and C_7, respectively, as illustrated in Fig. 4. All the assignments were in good agreement with previously studied systems. Thus, the sequence of peaks presented in the spectrum for the hybrid material confirms the sequence of carbons of the pendant groups obtained by the synthetic method employed in the synthesis of these kinds of hybrid materials [27].

The degree of immobilization on the surface was determined by considering the elemental analysis data. The new porous clay modified with the MPDET moiety bonded to the inorganic matrix polymer gave 11.32% of nitrogen, obtained from C.H.N. analysis as presented in Table 1. Based on this value, the corresponding amount of nitrogen content in the organic pendant molecule covalently bonded to backbone structure was calculated as 5.70 mmol g^{-1} of clay (d), which can be compared with other results obtained by similar reactions [21]. From the structural point of view, such syntheses have a great advantage due to the incorporation of pendant groups on a well-structured inorganic nanomaterial, disposing active potential sites to metal interaction for cation removal, simulating an effluent system, at the solid/liquid interface [22].

The BET surface areas of the natural and modified clay samples demonstrated that chemical modification caused the formation of micropores in the solid particles, resulting in a higher surface area, revealing 889.7 $m^2 g^{-1}$ for KLT_{MPDET} and relative to the natural KLT sample with 35.0 $m^2 g^{-1}$. The pore diameters change in the same direction, varying from 1.4 nm for the natural to 4.8 nm for the anchored clay. The textural properties of natural and modified kaolinite samples are reported in Table 1, which depends on particle size shape, and distribution of cracks and pores in the material, and therefore, cannot be represented as a general characteristic of particular type of material. The modified sample presented a unimodal distribution of pore sizes while KLT showed a bimodal distribution, as illustrated in Fig. 5a. The adsorption–desorption isotherms of gaseous nitrogen of the natural and modified kaolinite clays are type IV according to the I.U.P.A.C. classification and have an H1 hysteresis loop that is representative of materials with pore of constant cross-section [28]. The volume adsorbed for all isotherms at a relative pressure (P/P_0) of approximately 0.5, which represent capillary condensation of nitrogen within the uniform mesopore structure, as illustrated in Fig. 5b. These results are in accordance with finding from Shanmugharaj et al. [29], who found that the intercalation of trifunctional silane in smectites tended to be more successful in aqueous media that in ethylene glycol.

3.2. Effect of contact time and kinetic of adsorption

The main purpose in this study is to establish the ideal conditions of the adsorbent capacity, by considering the contact time of the solution at the solid/liquid interface. The adsorption data for metal ion uptake versus contact time for a fixed adsorbent amount are shown in Fig. 6a, giving identical abrupt increases in adsorption at low times before reaching the plateaus. According to these data, equilibrium is achieved at around 10 and 20 min for KLT and KLT_{MPDET}, respectively. However, to be sure on the best adsorption conditions at higher concentrations levels, to obtain equilibrium at the solid/liquid interface, all the experiments were carried out with 2 h of contact time. This short

Table 1
Textural proprieties of natural and modified kaolinite samples, C.H.N. analysis, and quantification of organic molecules anchored in the modified kaolinite samples.

Sample	Surface area – SA_{BET} ($m^2 g^{-1}$)	Micropore area ($m^2 g^{-1}$)	Average pore diameter (nm)	Pore volume ($cm^3 g^{-1}$)	C (%)	H (%)	N (%)	d ($mmol g^{-1}$)
KLT	35.0	10.0	1.1	0.08	–	1.25 ± 0.10	–	–
KLT_{MPDET}	889.7	38.1	4.8	0.30	21.32 ± 0.11	3.83 ± 0.11	11.32 ± 0.12	5.70 ± 0.12

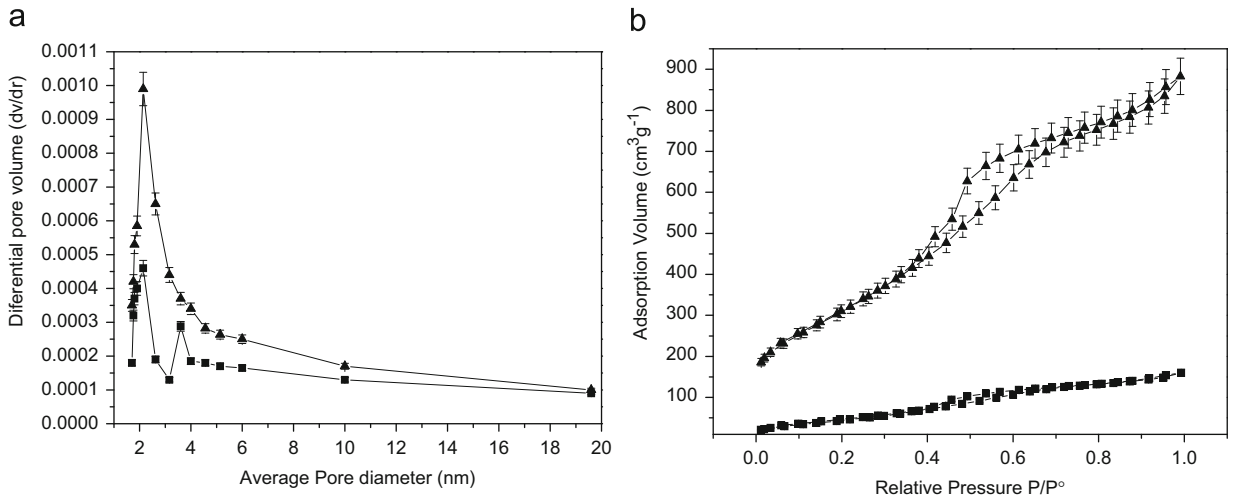

Fig. 5. Pore distribution of unmodified and modified kaolinite samples obtained by BJH method (a) and nitrogen adsorption–desorption isotherms of natural and modified kaolinite samples obtained BET method (b): ■, KLT and ▲, KLT_{MPDET}.

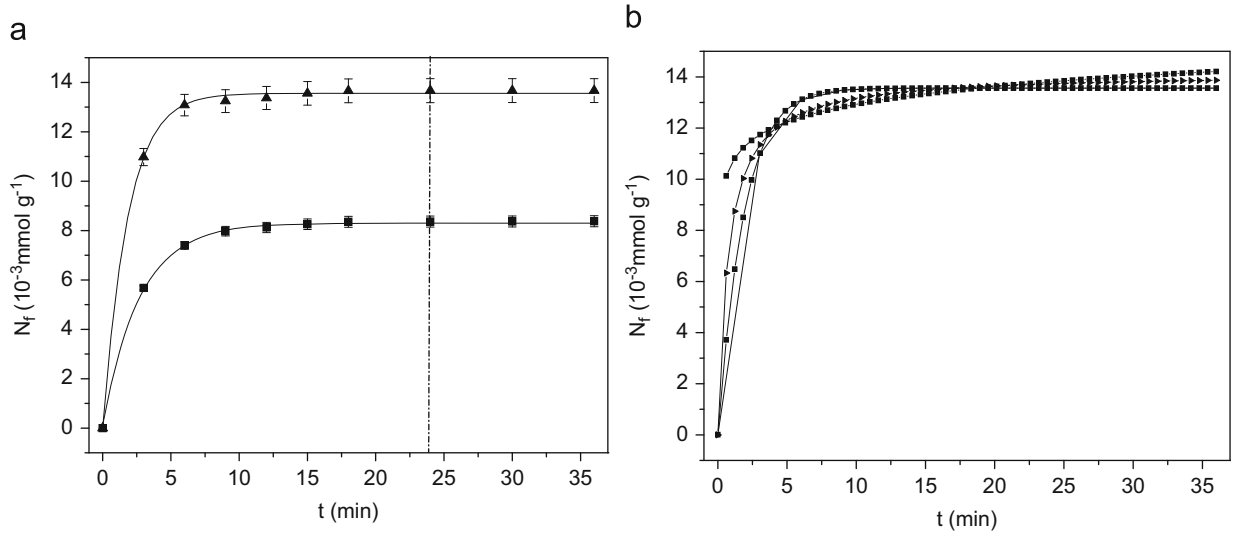

Fig. 6. Effect of contact time on the adsorption onto natural and modified kaolinite samples: ■, KLT and ▲, KLT_{MPDET} (a) and example of curve obtained by non-linear regression – KLT_{MPDET}/U(VI) (experimental – and calculated ■) (c) (clay 1.0 g dm^{-3}, pH 4.0, and controlled temperature in 298 ± 1 K).

time period required to attain equilibrium suggests an excellent affinity of the U(VI) for these adsorbents from aqueous solution. In order to study the specific rate constant of and U(VI)-phyllosilicates systems, was used a Lagergren pseudo-first-second-order and Elovich rate equations to simulate the kinetic adsorption of metal ion on the silicates, as illustrated in Fig. 6b.

Pseudo-first order kinetics using the Lagergren equation is generally expressed by Eq. (2) [30]:

$$\frac{\partial N_t}{\partial t} = k_1(N_{fEQ} - N_f) \quad (2)$$

After integration and applying the boundary conditions, $N_f = 0$ for $t = 0$ and $N_t = N_f$ at $t = t$, the integrated form of Eq. (2) becomes, Eq. (3):

$$\ln(N_{fEQ} - N_f) = \ln N_{fEQ} - k_1 t \quad (3)$$

where N_{fEQ} and N_f are the amounts of metal ion adsorbed at equilibrium and at a given time t ($mmol g^{-1}$), respectively, and k_1 is the rate constant for pseudo-first order adsorption (min^{-1}).

When the rate of reaction of an adsorption reaction is controlled by chemical exchange, then a pseudo-second order model can be better adjusted to the experimental kinetic data, as

expressed by Eq. (4):

$$\frac{\partial N_t}{\partial t} = k_2(N_{fEQ} - N_f)^2 \quad (4)$$

After integration and applying the boundary conditions, $N_f = 0$ for $t = 0$ and $N_t = N_f$ at $t = t$, the integrated form of Eq. (4) becomes, Eq. (5):

$$\frac{t}{N_t} = \left(\frac{1}{k_2 N_{fEQ}^2}\right) + \left(\frac{1}{N_{fEQ}}\right)t \quad (5)$$

where k_2 is the pseudo-second order rate ($mmol^{-1}\,min^{-1}$). The values of k_2 can be obtained from the y-intercept of the linear plot of t/N_f versus t.

Carrying out a set of experiments at constant temperature and monitoring the amount adsorbent with time, the kinetics of the adsorption process should be known. The adsorption using the Lagergren model can also be explored, as proposed in Eq. (2).

The useful Elovich equation for energetically heterogeneous solid surfaces is represented by Eqs. (6) and (7) in non-linear and linear forms, respectively [31]:

$$N_f = \ln(\alpha\beta t)^{\beta} \quad (6)$$

$$N_f = \beta \ln(\alpha\beta t) + \beta \ln t \quad (7)$$

where α and β, the Elovich coefficients, represent the initial adsorption rate ($mmol\,g^{-1}\,min^{-1}$) and the desorption coefficient ($g\,mmol^{-1}$), respectively.

When the rate of reaction of an adsorption reaction is controlled by chemical exchange, then a pseudo-second order model can be better adjusted to the experimental kinetic data [32]. Carrying out a set of experiments at constant temperature and monitoring the amount adsorbed with time, the kinetics of the adsorption process should be known. The kinetic constants values are shown in Table 2 for KLT and KLT_{MPDET}. The correlation coefficient of the pseudo-second-order rate equation (r^2) for the regression non-linear is 0.999, which suggests that the kinetic adsorption can be described by the pseudo-second-order rate equation very well.

3.3. Effect of concentration

The metal ion adsorptions on natural and chemically immobilized kaolinite samples are shown in Fig. 7a. The influence of the silylating agents covalently bonded on the inorganic structure is clearly reflected in adsorption isotherms due to different basic center attached to the pendant chains, as outlined by the saturation process [33–35]. The molecules anchored onto the oxides containing nitrogen basic atoms on pendant chains favor a metal ion interaction, mainly of soft cations, due to the presence of the basic reactive centers [35]. Based on the structural features presented by basic groups on the natural or modified clay surfaces, the adsorption can be related directly to the available nitrogen atoms. The Sips non-linear adsorption model was used to explain the significant capacity of these matrices to quantify uranyl interactions on these polymeric inorganic structures. The non-linear Sips model presents a significant advantage when used with such experimental data, allowing the determination of the capacity of cations bonded to basic centers and to evaluate the constant related to the binding energy. The large capacity of modified kaolinite sample was confirmed through constant values obtained with this model in the non-linear form, whose results gave the best approximation to the experimental data, as illustrated in Fig. 7b. The values are listed in Table 3. The large capacity of adsorption of the anchored kaolinite is represented by these constant values, which can be attributed to the immobilization of reactive basic groups on the pendant chains.

Table 2
Kinetics for pseudo-first order and pseudo-second order Lagergren and Elovich models calculated for U(VI) adsorption onto unmodified and modified kaolinite samples (clay 3.0 g dm^{-3}, initial U(VI) 25.0 mg dm^{-3}, pH 2.0, time 360 min and controlled temperature in 298 ± 1 K).

Sample	Pseudo-first order			Pseudo-second order			Elovich		
	$k_1 \times 10^2$ (min^{-1})	N_{fcal} ($mmol\,g^{-1}$)	r^2	$k_2 \times 10^3$ ($mmol\,g^{-1}\,min^{-1}$)	$\mathbf{N_{fcal}}$ ($mmol\,g^{-1}$)	r^2	$\alpha \times 10^3$ ($g\,mmol^{-1}\,mim^2$)	β ($mmol\,g^{-1}\,mim^{-1}$)	r^2
KLT	12.2 ± 0.2	7.8 ± 0.2	0.998	16.0 ± 0.2	8.5 ± 0.4	0.999	9.3 ± 0.1	10.2 ± 0.1	0.876
KLT_{MPDET}	22.1 ± 0.1	13.2 ± 0.4	0.989	25.1 ± 0.2	14.0 ± 0.2	0.999	24.5 ± 0.3	20.7 ± 0.1	0.887

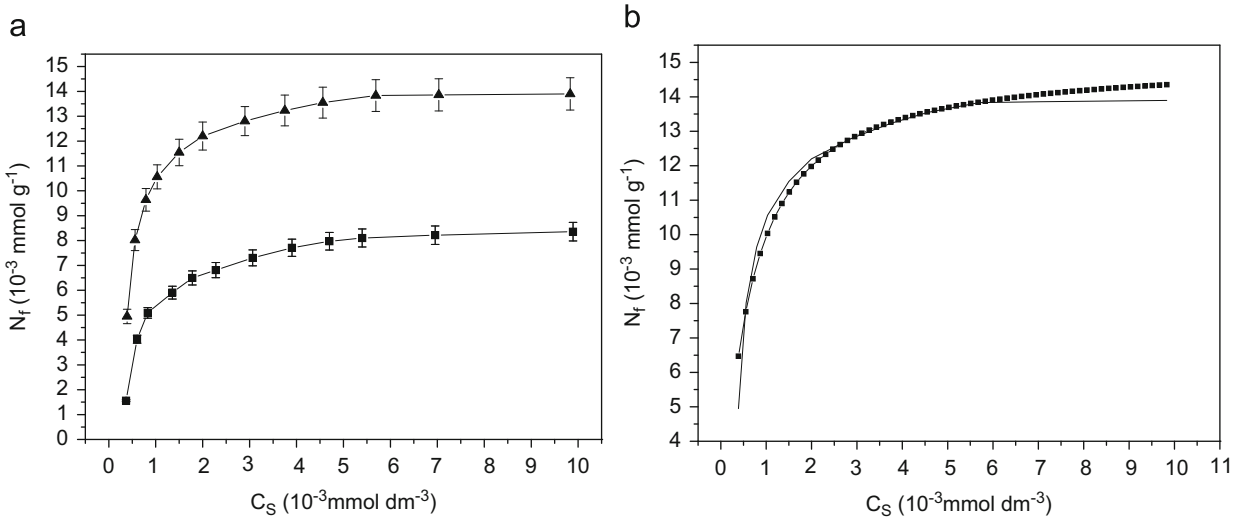

Fig. 7. Adsorption performance of natural and modified kaolinite samples in uranyl aqueous solution: KLT ■ and KLT_{MPDET} ▲ (a), experimentally adjusted data with Sips non-linear model, experimental (–) and calculated (■) curves (b) (clay 3.0 g dm^{-3}, pH 2.0, time 360 min, and controlled temperature in 298 ± 1 K).

Table 3
Thermodynamic data for U(VI) adsorption onto natural and modified kaolinite samples (clay 1.0 g dm^{-3}, pH 4.0, time 360 min, and temperature of 298 ± 1 K).

Sample	N_f^{max} [a] (10^{-3} mmol g^{-1})	N_f^{max} [b] (10^{-3} mmol g^{-1})	N_S (10^{-3} mmol g^{-1})	$-\Delta_{int}h$ (J g^{-1})	$-\Delta_{int}H$ (kJ mol^{-1})	n	$K_S \times 10^{-3}$	$-\Delta_{int}G$ (kJ mol^{-1})	$\Delta_{int}S$ (J K^{-1} mol^{-1})
KLT	8.37 ± 0.11	8.51 ± 0.09	8.72 ± 0.09	61.05 ± 0.14	7.61 ± 0.11	0.87	6.7 ± 0.1	21.9 ± 0.2	48 ± 1
KLT_{MPDET}	13.87 ± 0.11	13.89 ± 0.11	13.91 ± 0.11	94.68 ± 0.15	7.27 ± 0.02	0.99	10.4 ± 0.2	22.9 ± 0.1	53 ± 2

[a] Batch adsorption.
[b] Column adsorption: BP_1—lower breakpoint obtained after passing an effluent volume of 2.00×10^{-2} mmol dm^{-3} of U(VI) by the adsorbent column, the maximum amount allowed of the uranyl ion is surpassed. BP_2—higher breakpoint obtained after passing an effluent volume of 2.00×10^{-2} mmol dm^{-3} of U(VI) by the adsorbent column, the saturation of the adsorbent occurs.

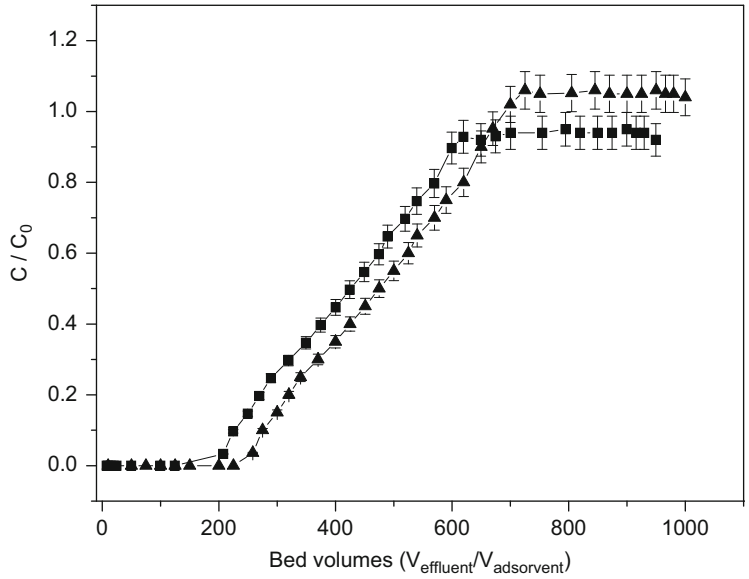

Fig. 8. Breakthrough curves for 2.00×10^{-2} mmol dm^{-3} of U(VI): KLT ■ and KLT_{MPDET} ▲ (clay 1.0 g dm^{-3}, pH 4.0, time 360 min, and controlled temperature in 298 ± 1 K).

Thus, the attached groups are the reactive basic center that contributes directly to the adsorption property of the anchored kaolinite sample.

The kaolinite cation adsorption capacity for two systems depends on the nature of the complex formed on surface and also on the affinity of the metal ion for any particular attached ligand [36]. The maximum cation adsorption capacity, N_f^{max}, for natural and organofunctionalized kaolinite clay samples is listed in Table 3; these values were obtained experimentally, and the higher adsorption capacity in the case of KLT_{MPDET} may be attributed to the organofunctionalization surface of KLT, showing also an increase with variation of uranyl concentration. These N_f^{max} values reflect the good affinity of the nitrogen donor atoms attached to the inorganic backbone for bonding uranyl. Favorable nitrogen/uranyl interactions were previously observed for these silylating agents when immobilized on kaolinite original sample [37]. These results are in accordance with finding from Guerra et al. [38,39], as observed from natural and modified clays present the same order of magnitude as those obtained with the synthetic Na-kanemite [38] ($N_f^{max} = 15.35$ and 19.48 mmol g^{-1}) and Hectorite clays [39] ($N_f^{max} = 7.86$ and 12.02 mmol g^{-1}) in adsorption process with U(VI), these matrices were chemically modified with N^1-propyldiethylenetrimethoxysilane and bis[3-(triethoxysilyl)propyl]tetrasulfide, in similar experimental conditions of the present investigation.

3.4. Adsorption study in dynamic conditions

In order to evaluate natural and modified kaolinite samples as absorbents for wastewater treatment of U(VI) containing effluents, breakthrough curves of this metallic ion using KLT and KLT_{MPDET} as absorbents were obtained, as illustrated in Fig. 8. In Table 3 were presented the lower (BP_1) and higher breakpoints (BP_2) of the breakthrough curves depicted in Fig. 8. As can be seen, the lower breakthrough points (BP_1), determined when the metallic ion effluents from column attained the concentration higher than 0.010 mg dm^{-3}. The BP_1 value is related with the capacity of the absorbents in retaining U(VI) ion from aqueous media. The higher breakpoints (BP_2) are related with the complete saturation of the kaolinite samples with the U(VI) ion. The values of BP_1 indicates that the natural and modified kaolinite samples are efficient absorbents for decontaminating radionuclide U(VI) from industrial effluents, using a dynamic system, since one volume of the adsorbent is able to remove completely at least 100 volumes of contaminated U(VI) ion from aqueous media. The saturations of the absorbents by U(VI) ion in dynamic conditions are depicted on Table 3. As can be seen, the maximum saturation of the natural and modified kaolinite samples by U(VI) using a dynamic adsorption system is very close to the values obtained in the batch adsorption experiments for two systems.

3.5. Thermodynamic study

From calorimetric titration data, the net thermal effects resulted in the corresponding well-behaved isotherms that were fitted to the Sips model, as shown in Fig. 9a. The respective curve for KLT_{MPDET} obtained with non-linear regression [14] is given in Fig. 9b. Complete sets of thermodynamic data for each system studied are listed in Table 3. As observed, cation/basic center

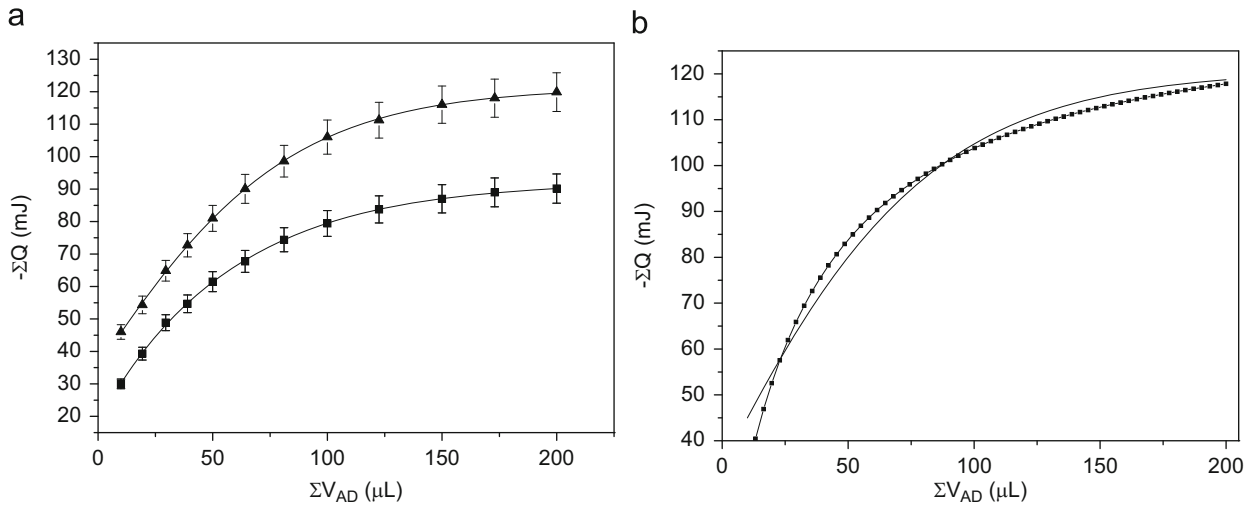

Fig. 9. The resulting thermal effects of the adsorption isotherms for the uranyl: KLT ■ and KLT_{MPDET} ▲ (a) and example of curve obtained by non-linear regression – KLT_{MPDET} /U(VI) (experimental – and calculated ■) (b) (clay 1.0 g dm^{-3}, pH 4.0, and time 8.0 h).

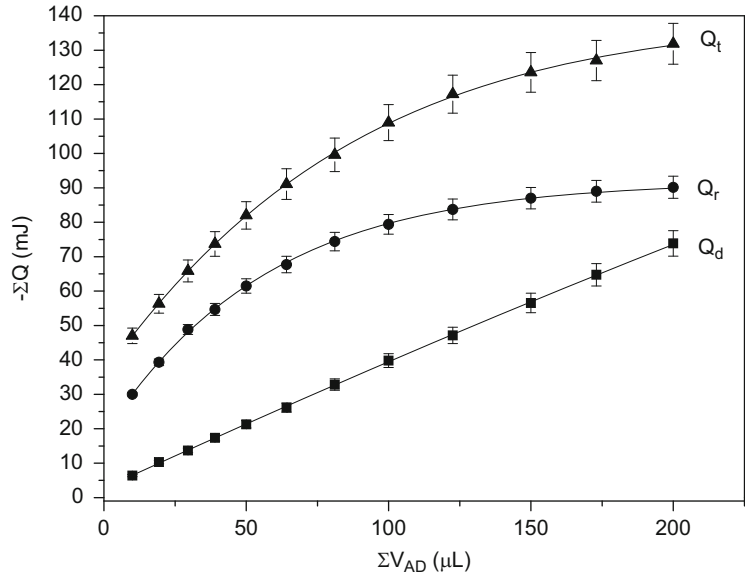

Fig. 10. The resulting thermal effect of adsorption U(VI) on modified kaolinite clay at 298 ± 1 K. The experiment points represent the thermal effect of cation titration $\sum Q_t$ (▲), cation dilution $\sum Q_d$ (■) and the net thermal effect of interaction $\sum Q_r$ (●), $\sum Q$, and V_{ad} values are the sum of detected thermal effect and total injected volume of U(VI) solution.

interactions for all system are spontaneous in nature as reflected their negative enthalpic values. The series of exothermic enthalpic data did not permit distinguishing a preference of any particular cation to bond with the available basic centers attached to the pendant groups covalently bonded to the inorganic backbone [40,41]. However, the positive entropic values for all interactions that contribute to the favorable interactive process are associated with solvent molecules displacement, initially bonded to the inorganic matrix, which is reinforced by desolvation of the cations before interacting with the basic centers. In such interactive processes the increase in free molecules in the reaction medium gives a positive entropy, thus demonstrating a favorable set of thermodynamic data for this kind of system [40,41]. An illustration of all the steps of calorimetric titration of 0.020 g of the original kaolinite (KLT) with 2.0×10^{-2} mmol dm^{-3} of U(VI) solution is shown in Fig. 10. This value was adjusted to the modified Langmuir model (Eq. (8)), which is

$$\frac{\sum X}{\sum \Delta_r H} = \frac{\sum X}{\Delta_{int} H} + \frac{1}{\Delta_{int} H (K_L - 1)} \tag{8}$$

where ΣX is the sum of the mole fraction of each cation in solution, after adsorption, obtained for each experimental point of titrand addition. $\Delta_r H$ is the integral enthalpy of adsorption for each point of the calorimetric titration obtained by dividing the thermal effect resulting from adsorption by the number of moles of adsorbate. K_L is the proportionality constant that also includes the equilibrium constant. $\Delta_{int} H$ is the thermal effect of formation of a monolayer on the surface.

Fig. 11 shows as an example, one of the titration thermograms obtained when KLT_{MPDET} adsorbs the U(VI) cation: it shows that, under the conditions applied, equilibrium is attained rapidly.

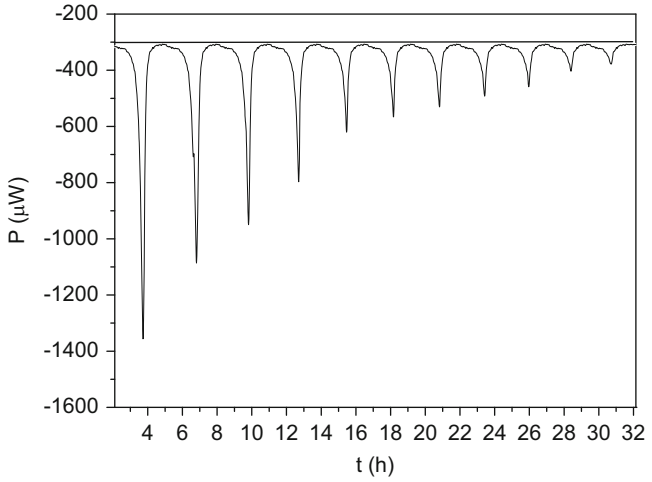

Fig. 11. Variation of the thermal effect versus time upon microcalorimetric titration of unmodified kaolinite sample (KLT) suspended in water with 20.0 cm^{-3} of uranyl cation at 298 ± 1 K (clay 3.0 g dm^{-3}, initial U(VI) 25.0 mg dm^{-3}, pH 2.0, and controlled temperature in 298 ± 1 K).

The integrated hest value is obtained by use of the data treatment Digitam 4.1 program (thermometric).

The Gibbs free energy, entropy, and enthalpy values are listed in Table 3. These values suggest that, during complex formation, desolvation disturbs the structure of the reaction medium to promote the disorganization of the system and, consequently, leads to an increase in entropy [38–41].

4. Conclusion

The immobilization of the N^1-[3-(trimethoxysilyl)propyl]-diethylenetriamine (MPDET) molecule onto phyllosilicate surface was obtained with success though heterogeneous routes. The material was characterized by various techniques confirming the formation of a hybrid material. The adsorption of the metallic ion depended on pH and shaking contact time. Adsorption on natural or modified kaolinite clay samples increased continuously with the concentration of uranyl. The metal ion adsorption studies onto the natural and modified kaolinite surfaces demonstrated that the inorganic–organic hybrid material can act as chelating agents in pollutant U(VI) ion removal from aqueous solution, where the maxima adsorption capacities are given by 8.37×10^{-3} and 13.87×10^{-3} mmol g^{-1} (batch adsorption). Batch and dynamic adsorption studies performed revealed that original and modified kaolinite clays could be successfully used as adsorbents for treating real industrial effluents containing U(VI).

The kinetics of adsorption of radionuclide used in this investigation on natural and organofunctionalized kaolinite samples were complex, but it seems that this interactive effect is better expressed by a pseudo-second order process. Non-liner regression method was compared to evaluate the experimental data with the pseudo-first-second order model and the Elovich model. Through calorimetric investigation information about all systems was obtained, resulting in exothermic enthalpy, negative Gibbs free energy and positive entropy. This series of thermodynamic data reflect the favorable cation/base center interaction at the solid/liquid interface.

Acknowledgments

The authors are indebted to CNPq for fellowships and FAPESP for financial support.

References

[1] A.R. Cestari, E.F.S. Vieira, A.J.P. Nascimento, F.J.R. Oliveira, R.E. Bruns, C. Airoldi, J. Colloid Interface Sci. 241 (2001) 45–51.
[2] F.A. Pavan, I.S. Lima, E.C. Lima, C. Airoldi, Y. Gushikem, J. Hazard. Mater. 137 (2006) 527–533.
[3] T. Murakami, T. Ohnuki, H. Isobe, T. Sato, Am. Miner. 82 (1997) 117–126.
[4] E.C. Pearcy, J.D. Prikryl, W.M. Murphy, B.W. Leslie, Appl. Geochem. 9 (1994) 713–732.
[5] C.E. Harland, Ion Exchange Theory and Practice, second ed, Royal Society of Chemistry, Cambridge, United Kingdom, 1994, p. 285.
[6] D.O. Cooney, Adsorption Design for Wastewater Treatment, Lewis Publishers, Boca Raton, 1999, p. 189.
[7] D.L. Guerra, A.A. Pinto, C. Airoldi, R.R. Viana, J. Solid State Chem. 181 (2008) 3374–3379.
[8] T.E. Payne, J.A. Davis, G.R. Lumpkin, R. Chisari, T.D. Waite, Appl. Clay Sci. 26 (2004) 151–162.
[9] X. Pang, F. Tang, Microporous Mesoporous Mater. 85 (2005) 1–6.
[10] G.S. Chamuah, S.K. Dey, Plant Soil 68 (2006) 135–138.
[11] S. Brunauer, P.H. Emmettt, E. Teller, J. Am. Chem. Soc. 60 (1938) 309–319.
[12] E.P. Barret, L.G. Joyner, P.P. Halenda, J. Am. Chem. Soc. 73 (1951) 373–380.
[13] D.L. Guerra, R.R. Viana, C. Airoldi, J. Colloid Interface Sci. 337 (2009) 122–130.
[14] D.L. Guerra, M.A. Carvallho, V.L. Leidens, A.A. Pinto, R.R. Viana, C. Airoldi, J. Colloid Interface Sci. 338 (2009) 30–39.
[15] R. Sips, J. Chem. Phys. 16 (1948) 490–495.
[16] I. Langmuir, J. Am. Chem. Soc. 40 (1918) 1361–1403.
[17] H.M.F. Freundlich, Z. Physik. Chemie. 57A (1906) 385–470.
[18] S. Lagergren, K. Suenk Vetenskapsakad. Handl. 241 (1898) 1–39.
[19] S.Z. Roginsky, J. Zeldovich, Acta Physicochim. 1 (1934) 554–594.
[20] C. Airoldi, L.N.H. Arakaki, J. Colloid Interface Sci. 249 (2002) 1–7.
[21] V.S.O. Ruiz, C. Airoldi, Thermochim. Acta 420 (2004) 73–78.
[22] A.M. Lazarin, C. Airoldi, Thermochim. Acta 454 (2007) 43–49.
[23] W.D. Keller, Clays Clay Miner. 26 (1978) 1–20.
[24] M. Zbik, R. Smart, Clays Clay Miner. 46 (2005) 153–160.
[25] D.L. Guerra, C. Airoldi, J. Braz. Chem. Soc. 20 (2009) 19–30.
[26] H.-J. Im, C.E. Barnes, S. Dai, Z. Xue, Microporous Mesoporous Mater. 70 (2004) 57–62.
[27] A.M. Liu, K. Hidajat, S. Kawi, D.Y. Zhao, Chem. Commun. (2000) 1145–1146.
[28] J. Jänchen, R.V. Morris, D.L. Bish, M. Janssen, U. Hellwig, Icarus 200 (2009) 463–467.
[29] A.M. Shanmugharaj, K.Y. Rhee, S.H. Ryu, J. Colloid Interface Sci. 298 (2006) 854–859.
[30] Y.S. Ho, G.M. McKay, Proc. Biochem. 34 (1999) 451–465.
[31] G.A. Taylor, N. Thon, J. Am. Chem. Soc. 74 (1952) 4169–4173.
[32] Y.S. Ho, D.A.J. Wase, C.F. Forster, Environ. Technol. 17 (1996) 71–77.
[33] B. Salih, A. Denizli, C. Kavakli, E. Pişkin, Talanta 46 (1998) 1205–1213.
[34] W. Xiu-Wen, M. Hong-Wen, L. Jin-Hong, J. Zhang, L. Zhi-Hong, J. Colloid Interface Sci. 315 (2007) 555–561.
[35] X. Tang, Z. Li, Y. Chen, J. Hazard. Mater. 161 (2009) 824–834.
[36] T.R. Macedo, G.C. Petrucelli, C. Airoldi, Clays Clay Miner. 55 (2007) 151–159.
[37] T.W. Weber, R.K. Chakraborty, J. Am. Inst. Chem. Eng. 20 (1974) 228–238.
[38] D.L. Guerra, A.A. Pinto, C. Airoldi, Inorg. Chem. Commun. 11 (2008) 20–23.
[39] D.L. Guerra, R.R. Viana, C. Airoldi, J. Environ. Radioact. 101 (2010) 122–133.
[40] R. Dey, C. Airoldi, J. Hazard. Mater. 156 (2008) 95–101.
[41] I.S. Lima, C. Airoldi, Thermochim. Acta 421 (2004) 133–139.